

Noninvasive bipolar double-pulsed-field-gradient NMR reveals signatures for pore size and shape in polydisperse, randomly oriented, inhomogeneous porous media

Noam Shemesh,¹ Evren Özarslan,² Tal Adiri,¹ Peter J. Basser,² and Yoram Cohen^{1,a)}

¹*School of Chemistry, The Raymond and Beverly Sackler Faculty of Exact Sciences, Tel Aviv University, Tel Aviv 69978, Israel*

²*Section on Tissue Biophysics and Biomimetics, NICHD, National Institutes of Health, Bethesda, Maryland, 20814 USA*

(Received 22 March 2010; accepted 24 May 2010; published online 22 July 2010)

Noninvasive characterization of pore size and shape in opaque porous media is a formidable challenge. NMR diffusion-diffraction patterns were found to be exceptionally useful for obtaining such morphological features, but only when pores are monodisperse and coherently placed. When locally anisotropic pores are randomly oriented, conventional diffusion NMR methods fail. Here, we present a simple, direct, and general approach to obtain both compartment size and shape even in such settings and even when pores are characterized by internal field gradients. Using controlled porous media, we show that the bipolar-double-pulsed-field-gradient (bp-d-PFG) methodology yields diffusion-diffraction patterns from which pore size can be directly obtained. Moreover, we show that pore shape, which cannot be obtained by conventional methods, can be directly inferred from the modulation of the signal in angular bp-d-PFG experiments. This new methodology significantly broadens the types of porous media that can be studied using noninvasive diffusion-diffraction NMR. © 2010 American Institute of Physics. [doi:10.1063/1.3454131]

I. INTRODUCTION

Characterizing morphological features of pores that are embedded within opaque porous media is of great significance in a wide variety of disciplines ranging from physical chemistry and geology to biomedicine. Restricted diffusion occurs when molecules diffusing within pores and interstices of a solid or a gel matrix encounter the boundaries of the restricting medium. When these molecules bear nonzero nuclear spin, magnetic resonance (MR) methods can be used to probe the porous medium noninvasively, with the fluid inside the pores serving as an endogenous reporter for pore morphology.^{1,2} Importantly, these morphological features provide a fingerprint of the pore space, and indeed diffusion MR methods are used to study pores in, *inter alia*, rocks,³ heterogeneous catalysts,⁴ porous materials,⁵ emulsion systems,⁶ and even biological cells⁷ and central-nervous-system (CNS) microstructures.^{1,8} In most of these applications, accurate determination of pore size and shape is crucial to completely characterize the porous media, and clearly nondestructive methodologies are preferable.

Conventional single-pulsed-field-gradient⁹ (s-PFG) [sequence shown in Fig. 1(a)] diffusion MR methods utilize a pair of diffusion gradients that sensitize the MR signal to molecular displacement during the time interval between the two gradients (Δ); the resulting signal decay is a manifestation of the diffusion processes that occur within the excited volume. The most widely employed s-PFG methodologies are diffusion tensor imaging¹⁰ (DTI), conducted at low

q-values, and q-space MR, conducted at higher q-values [where $\mathbf{q}=(2\pi)^{-1}\gamma\delta\mathbf{G}$, γ , δ , and \mathbf{G} are the gyromagnetic ratio, the gradient duration, and the gradient vector, respectively]. In DTI, the diffusion tensor is extracted and the tensor components yield measures of diffusion anisotropy.¹⁰ DTI has proven extremely useful for characterizing coherently placed anisotropic structures in normal^{11,12} and diseased¹³ CNS tissues.

The q-space approach utilizes the diffusion-diffraction patterns that are observed when higher q-values are reached to obtain compartmental dimensions.¹⁴ Importantly, the pore size can be directly derived from the minima of the signal decay provided that the geometry is known.^{14,15} Moreover, these diffusion-diffraction patterns¹⁴ bear a signature for restricted diffusion and are thus very informative.¹⁴ Indeed, diffusion-diffraction patterns were experimentally observed in relatively monodisperse specimens such as red blood cells¹⁶ and narrowly distributed emulsions.⁶

The major *caveat* of the abovementioned approaches is that they yield microstructural information only when pores are coherently ordered and relatively monodisperse in size, whereas most porous media are characterized by more heterogeneous attributes. Many porous media including, *inter alia*, gray matter in the CNS, porous polymers, liquid crystals, heterogeneous catalysts, and porous rocks are characterized by locally anisotropic pores that are randomly oriented and have size distributions, where the diffusion-diffraction minima vanish from the s-PFG signal decay; thus, the microstructural information is limited or, in fact, lost.

A further complication is the presence of strong internal magnetic field gradients^{3,17} that arise from susceptibility dif-

^{a)}Author to whom correspondence should be addressed. Electronic mail: ycohen@post.tau.ac.il. Tel.: 972 3 6407232. FAX: 972 3 6407469.

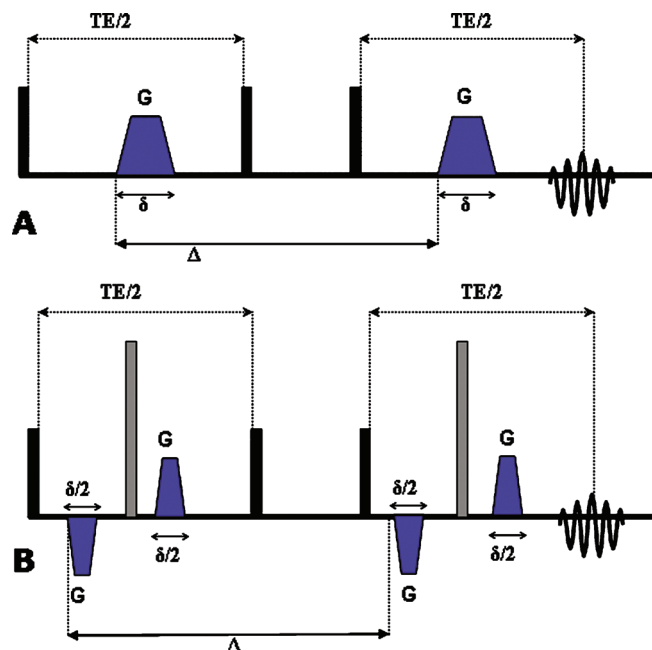


FIG. 1. s-PFG sequences. (a) The single-stimulated echo (s-STE) sequence. (b) The bipolar s-STE. Δ —diffusion period, δ —gradient duration, and TE—echo time. Black and gray boxes represent $\pi/2$ and π rf pulses, respectively.

ferences within the porous medium.^{18,19} The deleterious nature of susceptibility-induced internal magnetic field gradients²⁰ exacerbate the loss of diffusion-diffraction minima even in coherently placed pores, rendering the pore size intractable directly from the signal decay.²¹ These drawbacks prohibit accurate characterization of heterogeneous po-

rous media using s-PFG methods and indirect and complicated methods of analysis of the signal decay then need to be employed.^{3,22}

In this study we present a simple yet general method to overcome these limitations using double-PFG (d-PFG) methodology,²³ hybridized with bipolar gradients that partially suppress internal magnetic field gradients that are prominent in most chemical and geological applications. The d-PFG methodology employs a second gradient pair, which is separated from the first pair by a mixing time (t_m) [Fig. 2(a)] that can be effectively set to zero by superposing the middle gradients [Fig. 2(b)]. Previous studies on other variants of d-PFG (which was first introduced in Ref. 23) focused on two-dimensional experiments,²⁴ convection artifacts suppression,²⁵ and even on studying pore eccentricity in yeast²⁶ and locally anisotropic motion in liquid crystals.²⁷ Recently, the d-PFG methodology gained interest in MR theory,^{28–31} spectroscopy,^{32–35} and imaging.^{36–40}

Recent progress in theory suggested that the d-PFG methodology may be advantageous over current s-PFG methodologies in characterizing pore size and shape owing to several inherent attributes of d-PFG even when locally anisotropic pores are polydisperse or randomly oriented. Notably, zero-crossings in the signal decay in d-PFG that are analogous to diffusion-diffraction minima in s-PFG were predicted to be more robust toward size polydispersity.²⁸ In a recent study, these theoretical predictions were experimentally demonstrated on controlled specimens comprised of water-filled coherently placed microcapillaries with increasing polydispersity.³⁵ It was experimentally shown that the

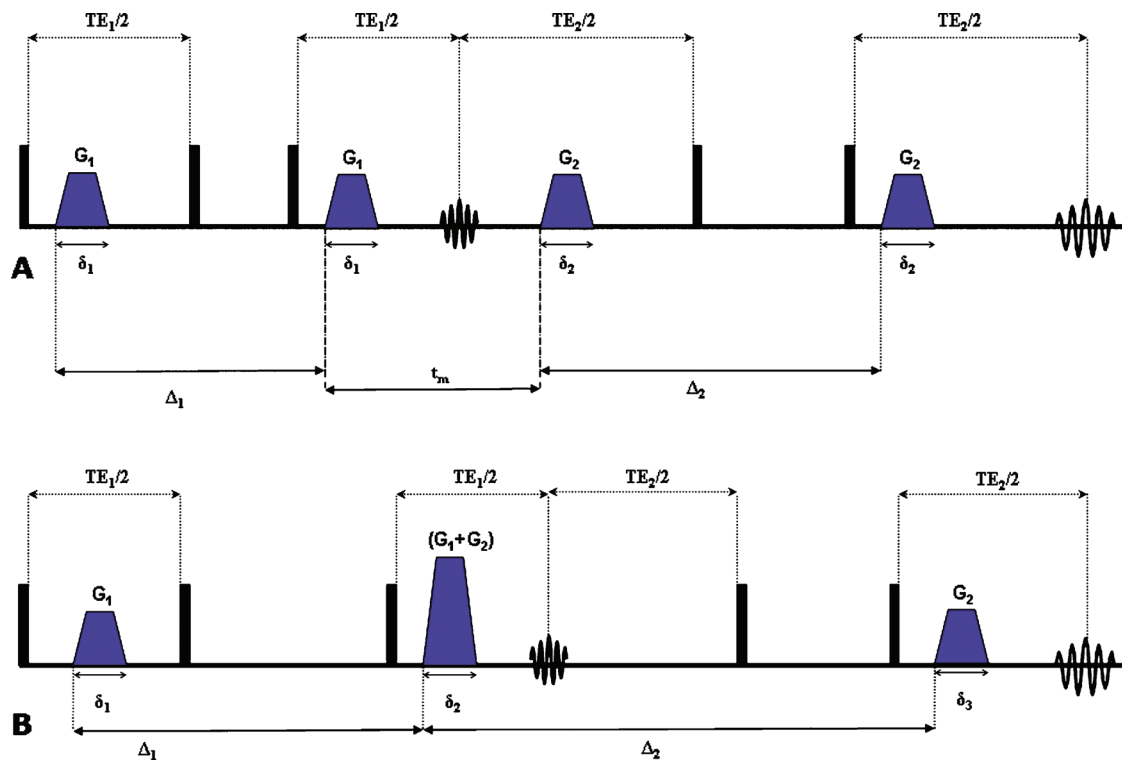


FIG. 2. d-PFG sequences. (a) The double-stimulated echo (d-STE) sequence with finite mixing time. (b) The d-STE sequence with zero mixing time. Δ —diffusion period, δ —gradient duration, TE—echo time, and t_m —mixing time. Black boxes represent $\pi/2$ rf pulses.

zero-crossings persisted in d-PFG NMR even for relatively broad size distributions, while the diffusion-diffraction patterns in s-PFG vanished.³⁵ The zero-crossings in d-PFG NMR offered novel microstructural information since the q -value of zero-crossing was indicative, at least qualitatively, of the average size of the pores, and the rate of return to the ambient noise level was found to give a good indication of the width of the distribution, parameters which could not be directly inferred from the s-PFG experiments.

Recent theoretical progress suggested that the zero-crossings in d-PFG should persist even when locally anisotropic pores are randomly distributed.²⁹ Notably, this implies a new way to characterize such specimens in terms of pore size, a major advantage for d-PFG, since diffusion-diffraction patterns vanish from the signal decay in s-PFG when specimens are polydisperse in size or shape^{28,35,41} and resorting to model-dependent and sophisticated methods^{3,42} is necessary to obtain microstructural information.

Another advantage of d-PFG is that local pore shape can be derived from the angular d-PFG experiment, first proposed theoretically by Mitra.⁴³ The theory predicts that when the angle between the gradients (denoted by ψ) is varied at long mixing times (t_m), the $E(\psi)$ curves at different q -values are a manifestation of compartment shape anisotropy.²⁹ This information on local anisotropy is unique to d-PFG and cannot be inferred by conventional s-PFG methods since the angle ψ is inherently unique to the angular d-PFG methodology.

In this study, we extend the findings in Ref. 35 (persistence of zero-crossings in size distributions) to randomly oriented anisotropic pores and show that, indeed, the zero-crossings in the hybrid bipolar-d-PFG (bp-d-PFG) methodology persist in controlled heterogeneous porous media even in the presence of severe internal magnetic field gradients and random orientation of locally anisotropic pores. Moreover, we show for the first time that compartment shape anisotropy can be observed at long mixing times using the angular d-PFG methodology and that the local compartment shape can be easily inferred from such measurements even when pores are randomly oriented. Thus, the bp-d-PFG methodology is capable of characterizing porous media that have all degrees of complexity found in nature (random orientation of locally anisotropic pores, size polydispersity, and internal magnetic field gradients) and which are extremely hard to characterize using conventional methods.

II. MATERIALS AND METHODS

A. Specimen preparation

Hollow microcapillaries with well defined inner diameter (ID) (PolyMicro Technologies, Phoenix, AZ) were immersed in distilled water for several days prior to each experiment. The water-filled microcapillaries were manually cut to very small pieces (<0.5 cm) and then crushed by mechanical force to “dustlike” small particles. In some cases, the microcapillaries were not crushed but only cut into very small pieces that enabled random orientation within the NMR tube. The resulting porous medium was reimmersed in water for several days to refill. The porous crush was then

poured to an 8 mm or in some cases 10 mm NMR tube containing Fluorinert (Sigma-Aldrich, Rehovot, Israel). The Fluorinert served, owing to density and polarity differences, to keep any extratubular water in the top part of the NMR tube, which was located outside the rf coils.

The polydisperse specimen was prepared in the same way, only instead of using monodisperse microcapillaries, a mix of microcapillaries of varying sizes was used. Specifically, we used the specimen denoted SD003 in a recently published study,³⁵ which encompasses microcapillaries with five different IDs. The mean \pm stdv ID of this specimen is 14.9 ± 4.6 μm .

B. Scanning electron microscope experiments

Characterization of the morphology and orientation of the porous media was performed using high resolution scanning electron microscope (SEM) (JEOL 6700F operated at 15 keV, Tokyo, Japan) equipped with a secondary-electron detector.

C. NMR experiments

The NMR tube containing the porous medium was placed in a Bruker 8.4 T NMR spectrometer (Karlsruhe, Germany) equipped with a Micro5 probe capable of producing nominal pulsed gradients up to 1900 mT/m in each direction. The temperature was kept constant throughout the experiments. The length of the hard $\pi/2$ pulses in all specimens was 15 ± 1 μs .

D. Randomly oriented pores with ID=29 \pm 1 μm

The s-PFG and bp-s-PFG were conducted using the sequences shown in Figs. 1(a) and 1(b) respectively, with the following parameters: $\Delta/\delta=250/3$ ms, 32 q -values were collected with G_{max} of 600 mT/m, resulting in a maximum q -value of 766 cm^{-1} . The number of scans was set to 32.

The d-PFG and bp-d-PFG experiments were performed using the sequences shown in Figs. 2(b) and 3(b), respectively, and with the following parameters: $\Delta_1=\Delta_2=250$ ms, $\delta_1=\delta_2=\delta_3=3$ ms, and $t_m=0$ ms. A total of 32 points was collected with $G_{\text{max}}=300$ mT/m, resulting in a q_{max} of 383 cm^{-1} .

E. Randomly oriented pores with ID=19 \pm 1 μm

The s-PFG and bp-s-PFG were conducted with the sequences shown in Figs. 1(a) and 1(b), respectively, $\Delta/\delta=200/3$ ms, and with G_{max} of 800 mT/m, resulting in a maximum q -value of 1022 cm^{-1} .

The d-PFG and bp-d-PFG experiments were performed using the sequences shown in Figs. 2(b) and 3(b), respectively, and with the following parameters: $\Delta_1=\Delta_2=200$ ms, $\delta_1=\delta_2=\delta_3=3$ ms, and $t_m=0$ ms. A total of 24 q -values was collected with $G_{\text{max}}=400$ mT/m, resulting in a q_{max} of 510.5 cm^{-1} .

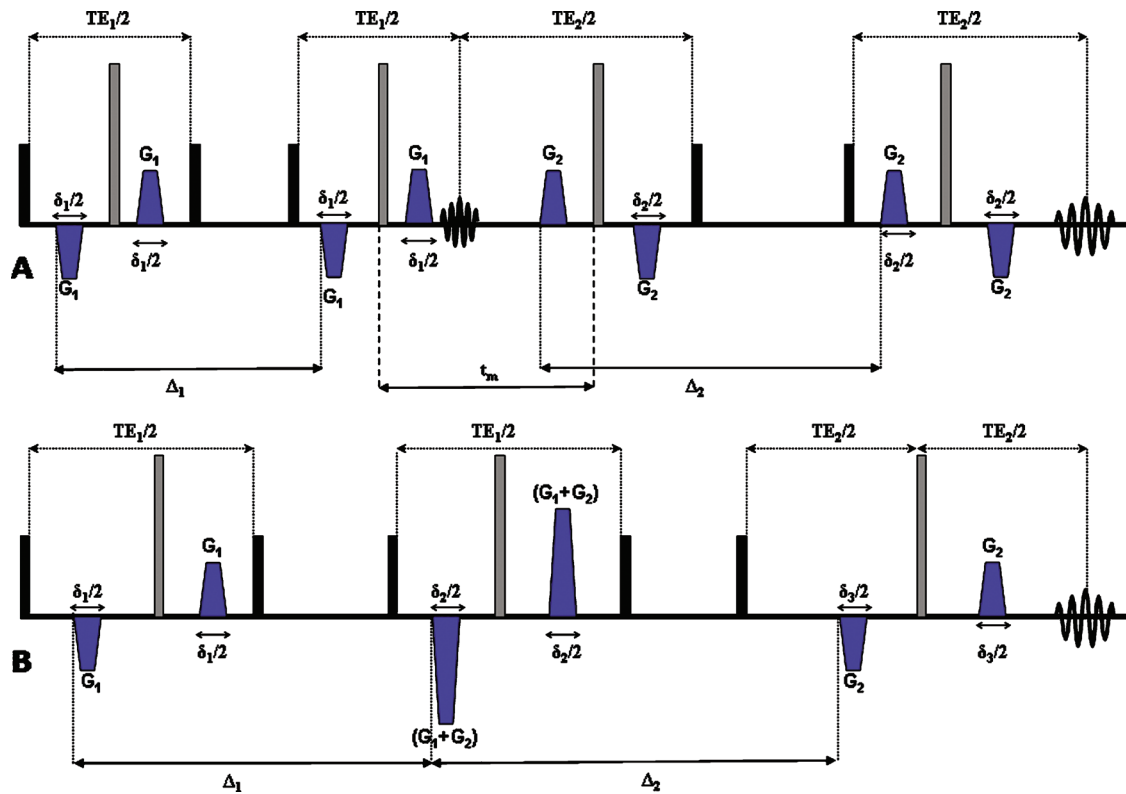


FIG. 3. bp-d-PFG sequences. (a) The bipolar-d-STE (bp-d-STE) sequence with finite mixing time. (b) The bp-d-STE sequence with zero mixing time. Δ —diffusion period, δ —gradient duration, TE—echo time, and t_m —mixing time. Black and gray boxes represent $\pi/2$ and π rf pulses, respectively.

F. Randomly oriented polydisperse pores

The s-PFG and bp-s-PFG were conducted with the sequences shown in Figs. 1(a) and 1(b), respectively, with $\Delta/\delta=150/3$ ms, and 32 q-values were collected with G_{\max} of 1600 mT/m, resulting in a maximum q-value of 2043 cm^{-1} .

The bp-d-PFG experiments were performed using the sequences shown in Figs. 2(b) and 3(b), respectively, and with the following parameters: $\Delta_1=\Delta_2=150$ ms, $\delta_1=\delta_2=\delta_3=3$ ms, and $t_m=0$ ms. A total of 32 q-values was collected with $G_{\max}=800$ mT/m, resulting in a q_{\max} of 1021.5 cm^{-1} .

G. Randomly oriented pores with $ID=10\pm 1 \mu\text{m}$

To show compartment shape anisotropy, the angular bp-d-PFG experiments were performed as described previously,^{20,22,24} with the sequences shown in Figs. 2(a) and 3(a) with the following parameters: $\Delta_1=\Delta_2=150$ ms, $\delta_1=\delta_2=3$ ms, and $t_m=18$ ms. Briefly, G_1 was fixed in the x-direction, and the orientation of G_2 was varied in 25 equal steps along 360° in the X-Y plane (perpendicular to the direction of B_0). In these angular d-PFG experiments $|G_1|=|G_2|$.

III. RESULTS

To establish the validity of the new approach toward characterizing pore size and shape, controlled porous media (Fig. 4) were used in which the ground truth is known *a priori*. Indeed, the SEM images of our porous medium phantom (Fig. 4) demonstrate that the pores are randomly

oriented [Fig. 4(a)], while Figs. 4(b) and 4(c) show their local cylindrical geometry. The NMR linewidth in these specimens was ~ 0.5 kHz, indicating the inhomogeneity of the sample, a manifestation of the relatively large susceptibility effects arising from the random orientation of the cylindrical pores.

A. Zero-crossings in monodisperse, locally anisotropic pores

To determine the microstructural information that can be extracted, s-PFG and d-PFG experiments were performed on a controlled monodisperse porous medium with randomly oriented cylindrical pores. To overcome the large

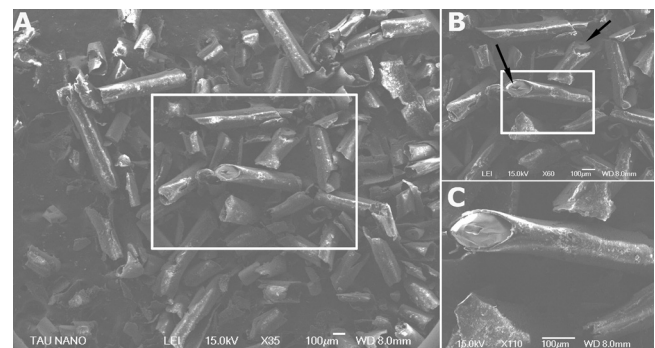


FIG. 4. SEM images of a representative porous medium used in this study. (a) The random orientation of the pores is apparent. (b) Magnification of the white box in (a) shows the local cylindrical geometry of the pores. (c) Magnification of the white box in (b). The ID of the cylinders (arrowheads) measured from these images was found to be $\sim 28 \mu\text{m}$, in good agreement with the nominal size for this specimen.

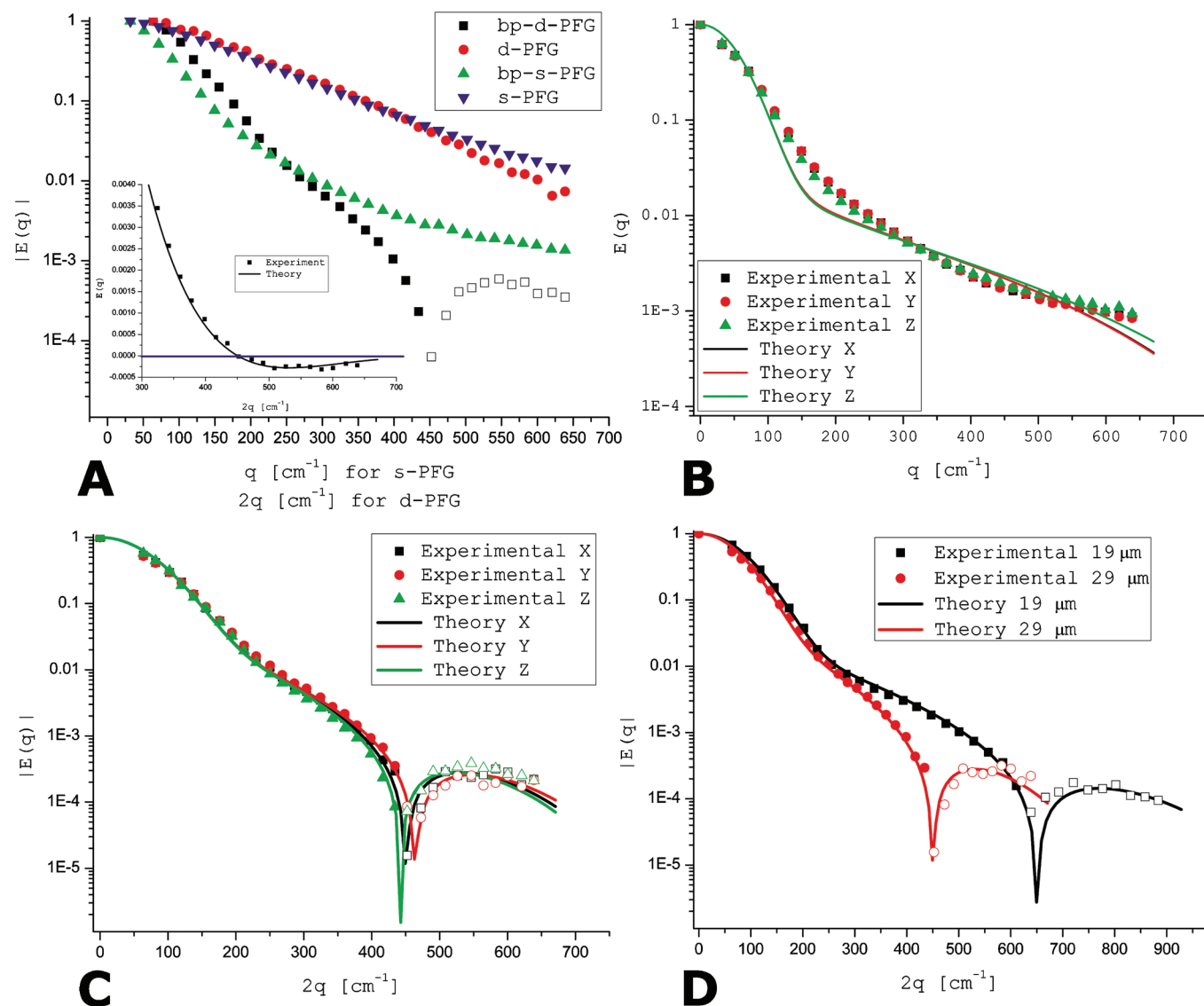


FIG. 5. Diffusion MR experiments in randomly oriented cylindrical pores characterized by a large internal magnetic field inhomogeneity. (a) s-PFG, bp-s-PFG, d-PFG, and bp-d-PFG experiments conducted on randomly oriented, locally cylindrical porous media with a nominal ID of $29 \pm 1 \mu\text{m}$. While s-PFG, d-PFG, and bp-s-PFG yield monotonic and featureless decays, the bp-d-PFG clearly demonstrates a zero-crossing (inset), which is manifested as a diffusion-diffraction minimum when $|E(q)|$ is plotted against the q -values. The theoretical curve (solid line, inset) agrees very well with the experimental points. (b) bp-s-PFG experiments in the x -, y -, and z -directions clearly demonstrate an isotropic signal decay, thus providing evidence that the pores are indeed randomly oriented. (c) The bp-d-PFG experiments also reveal an isotropic profile, and zero-crossings are observed in all spatial directions at a similar q -value. (d) Comparison of bp-d-PFG signal decay in randomly oriented porous media characterized by pores with $\text{ID}=29 \pm 1$ and $19 \pm 1 \mu\text{m}$. The zero-crossing for the $19 \pm 1 \mu\text{m}$ specimen, manifested as a diffractionlike minimum in the magnitude calculated plot, is observed at a higher q -value, as expected. Full symbols represent positive-valued signal, while empty symbols represent negative-valued signals.

susceptibility-induced internal fields, bipolar s-PFG and d-PFG sequences (denoted as bp-s-PFG and bp-d-PFG, respectively) were implemented [the sequences are shown in Fig. 1(b) and Fig. 3, respectively]. Introducing bipolar gradients and carefully timing the sequences has been previously shown to partially suppress the effects of deleterious background gradients and internal magnetic field gradients^{20,44} and even to restore diffusion-diffraction patterns when pores were coherently placed in an inhomogeneous field.²¹

Figure 5(a) shows the experiments performed on a controlled porous medium with nominal $\text{ID}=29 \pm 1 \mu\text{m}$ shown in Fig. 4. The s-PFG data are plotted against q , while d-PFG data are plotted against $2q$ for easy comparison.³⁴ The ex-

periment performed using the s-PFG sequence shown in Fig. 1(a) yielded a featureless decay, which was clearly affected by the large susceptibility artifact. The signal in bp-s-PFG experiments [sequence shown in Fig. 1(b)] attenuated somewhat more than in the s-PFG experiments; however, diffusion-diffraction troughs were not observed [Fig. 5(a)]. When d-PFG experiments were performed using the sequence shown in Fig. 2(b), the signal decay was again featureless and no microstructural information could be obtained directly from these $E(2q)$ plots.

By contrast, the signal decay in bp-d-PFG [sequence shown in Fig. 3(b)] is dramatically different: it clearly reveals the zero-crossings (manifested as diffusion-diffraction troughs when $|E(2q)|$ is plotted) arising from restricted dif-

fusion within the constituent pores [Fig. 5(a)]. The inset shows the actual zero-crossing, occurring at $2q=452\text{ cm}^{-1}$, and shows that indeed the signal turns to negative values at q -values greater than the zero-crossing. This is manifested as an inverted peak in the actual NMR signal decay.³² The signal decay was fitted to the theory,³¹ and the size that was obtained was $28.00 \pm 0.03\ \mu\text{m}$, in excellent agreement with the nominal ID of the pores ($29 \pm 1\ \mu\text{m}$).

To show that the pores are indeed randomly oriented, both bp-s-PFG and bp-d-PFG experiments were performed in the x -, y -, and z -directions. Figures 5(b) and 5(c) show the absolute values of the signal decay of bp-s-PFG and bp-d-PFG, respectively. The bp-d-PFG clearly demonstrates a zero-crossing (manifested as a diffusion-diffraction trough in the absolute valued plot) in all directions at similar q -values, while in bp-s-PFG, the diffusion-diffraction minima are absent for all directions. The isotropic signal decay implies that there is no preference for a certain orientation of the pores within the NMR tube, and that the pores in the specimen are indeed completely randomly oriented.

To show the sensitivity of the zero-crossings toward compartment size, similar experiments were performed on monodisperse porous media with a nominal ID of $19 \pm 1\ \mu\text{m}$ [Fig. 5(d)]. The zero-crossing is easily observed in this specimen too, and the location of the zero-crossing is indeed at a higher q -value of 632 cm^{-1} , as expected from smaller pores. Fitting to the theory yielded a compartment size of $19.65 \pm 0.20\ \mu\text{m}$, in excellent agreement with the nominal compartment size. The s-PFG, d-PFG, and bp-s-PFG experiments did not yield any diffusion-diffraction minima for all specimens studied, and only a smooth, non-monoexponential decay was observed, from which accurate microstructural information could not be directly inferred from the signal decay. Note that owing to the large internal gradients, the signal decays of both monopolar s- and d-PFG yield similar signal decays. By contrast, the signal decay in bp-s-PFG seems to follow the expected smooth attenuation form for randomly oriented anisotropic pores.

B. Zero-crossings in polydisperse, locally anisotropic pores

The results shown in Fig. 5 unequivocally demonstrate that bp-d-PFG can characterize randomly oriented monodisperse pores in terms of size even in the presence of internal magnetic field gradients; however, most porous media are also characterized by size polydispersity, which in itself results in the loss of diffusion-diffraction troughs in s-PFG even when pores are coherently placed.²⁸ In a previous study,³⁵ we were able to demonstrate that the zero-crossings in d-PFG persist in coherently placed polydisperse pores, while diffusion-diffraction minima vanished in s-PFG, thus demonstrating the clear advantage of d-PFG for characterizing polydisperse specimens.

To show that bp-d-PFG can indeed characterize porous media with all the degrees of complexity (i.e., inhomogeneous field, randomly oriented anisotropic pores, and size polydispersity), we used a polydisperse specimen having a mean \pm stdv of $14.9 \pm 4.6\ \mu\text{m}$,³⁵ which was cut into small

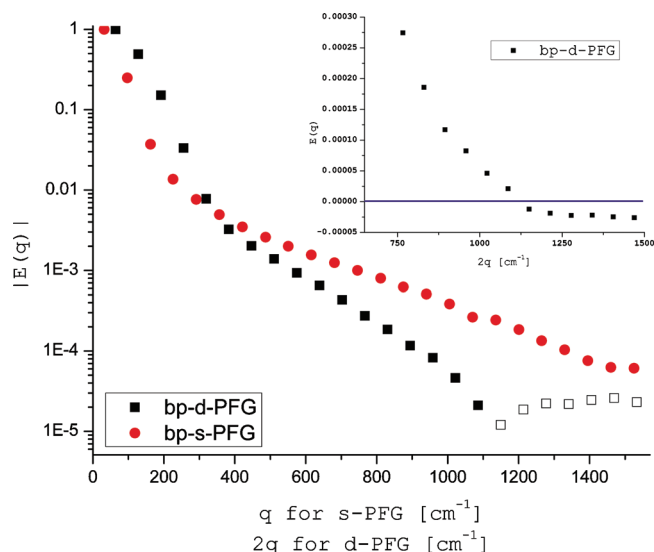


FIG. 6. Diffusion MR experiments in polydisperse randomly oriented cylindrical pores characterized by a size distribution of mean \pm stdv of $14.9 \pm 4.6\ \mu\text{m}$. Here, the bp-d-PFG yields a sharp zero-crossing, while bp-s-PFG shows a featureless decay. Full symbols represent positive-valued signal, while empty symbols represent negative-valued signals.

pieces to achieve a random orientation of the locally anisotropic pores. The bp-s-PFG and bp-d-PFG experiments on this specimen are shown in Fig. 6. Clearly, the bp-s-PFG does not yield diffusion-diffraction minima in this polydisperse porous medium; however, the zero-crossing of the bp-d-PFG indeed persists (inset) and is located at $2q = 1150\text{ cm}^{-1}$, corresponding to a compartment size of $10.6\ \mu\text{m}$, in good agreement with the nominal peak of the distribution, subject to a slight violation of the short gradient pulse approximation.³⁵ By contrast, the bp-s-PFG experiments yielded no diffusion-diffraction patterns, and microstructural information could not be obtained directly from the signal decay (Fig. 6). It should be noted that as in the previous monodisperse specimens, zero-crossings were not observed when d-PFG with monopolar gradients was performed (data not shown).

C. Extracting compartment shape in randomly oriented locally anisotropic pores

In the previous sections, the zero-crossings in bp-d-PFG experiments were shown to enable accurate extraction of compartment size; however, the local compartment shape could not be inferred directly from these $E(q)$ plots, as the zero-crossings appear isotropic. In fact, inspecting just the $E(q)$ plots in bp-d-PFG might lead to the erroneous conclusion that the pores are spherical! However, the theory predicts that compartment shape can be inferred from the angular d-PFG experiment, in which the angle ψ between the gradient pairs is varied at a long mixing time (t_m).^{29,43}

To explore the local shape of the pores, randomly oriented cylindrical pores with nominal ID = $10 \pm 1\ \mu\text{m}$ were used and the angular d-PFG experiment was performed using the bp-d-PFG sequence with long mixing times [sequence shown in Fig. 3(a)]. Figure 7 clearly reveals the characteristic $E(\psi)$ modulated curves, shown for two different q -values,

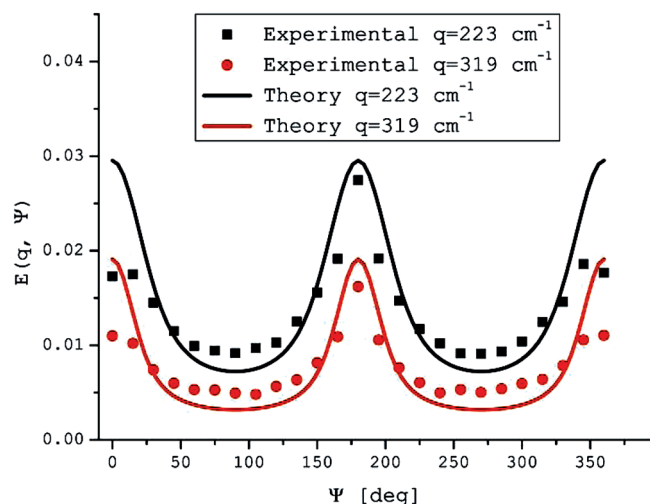


FIG. 7. Angular bp-d-PFG experiments performed on randomly oriented cylindrical pores with $ID=10 \pm 1 \mu\text{m}$. The finite t_m in these experiments causes compartment shape anisotropy to be accentuated, as manifested in the modulated angular signal. Such modulation is expected, e.g., for ellipsoidal or cylindrical pores, as opposed to a completely flat angular profile for spherical pores. These $E(\psi)$ modulations therefore are used to infer on local pore anisotropy even though the pores are completely randomly oriented within the specimen.

indicating that pores are indeed nonspherical. The distinctive shape of the modulated $E(\psi)$ curve is completely different from what is expected from spherical pores [where $E(\psi)$ is completely flat, i.e., there is no angular dependence at long t_m].²⁹ Therefore, it is easy to infer on the cylindrical nature of the pores. The theory and experiments are in good agreement, and a compartment dimension of $8.0 \pm 0.7 \mu\text{m}$ is extracted from fitting the angular dependence to the theory. The slight variation between theoretical and nominal size probably arises from incomplete suppression of susceptibility artifacts. Importantly, this is the first experimental observation of compartment shape anisotropy, which provides unique information on pore shape noninvasively, unavailable by any other method. It should be noted that when the angular d-PFG experiment was performed with the d-PFG experiment with monopolar gradients, the $E(\psi)$ profile was severely affected by the susceptibility effects, and the pore shape could not be obtained (data not shown).

IV. DISCUSSION

In this study, we presented a simple yet general approach for noninvasively characterizing morphological features of pores in opaque porous media even when most levels of complexity found in nature, namely, size polydispersity, random orientation of locally anisotropic pores, and magnetic field inhomogeneity, are present. Such a setting, although prominent in many porous media in a range of scientific disciplines ranging from biomedicine, geology, and chemistry to materials science, is extremely hard to characterize directly and noninvasively using conventional methods. Indeed, a method that would provide direct and robust characterization of pore shape and size would be advantageous over other model-dependent methodologies.

Our approach utilized bipolar gradients to overcome susceptibility-induced effects within the porous medium, hybridized with the d-PFG methodology which can convey pore size and shape even when specimens are heterogeneous in size and orientation. Therefore, the bp-d-PFG methodology uniquely yields noninvasive signatures for pore size and shape: the zero-crossings yield the pore size with very high accuracy and the $E(\psi)$ profiles obtained from angular bp-d-PFG experiments enables one to noninvasively obtain a signature for compartment shape. In most applications, knowledge of these morphological features is sufficient to completely characterize the porous medium noninvasively and provides a fingerprint for the specimen. It should be emphasized that even when we used the bipolar gradients in all s-PFG methodologies, we did not observe any diffusion-diffraction patterns, thus we could not directly derive the pore size from the signal decay. In all specimens, the bp-s-PFG yielded an isotropic signal decay, thus the local pore anisotropy could not be inferred. Interestingly, in the randomly oriented specimens, which are characterized by large magnetic field inhomogeneity, the bp-s-PFG exhibited a signal decay, which is much closer to its expected form than the s- or d-PFG experiments. Clearly, this occurs since the susceptibility effects in these specimens are rather dramatic, and the internal gradients dominate the signal decay to a large extent when monopolar gradients are used; these experiments demonstrate the importance of using bipolar gradients in both methodologies.

The zero-crossings are a manifestation of restricted diffusion in d-PFG NMR. Their robustness toward heterogeneity in both size and in shape arises from the fact that the signal is allowed to take a negative value in d-PFG NMR. Spins diffusing in compartments with different orientations contribute different signal values to the overall signal at each q -value. The fractional contribution of negative and positive signals leads to the cancellation of the signal at the q -value of the zero-crossing and thus to the persistence of the zero-crossings in d-PFG NMR. By contrast, the signal decay due to restricted diffusion in s-PFG is inherently always positive, and in the presence of randomly oriented anisotropic compartments, the additive nature of the signal simply smoothes the decay, leading to a loss of diffusion-diffraction minima. The robustness of d-PFG toward heterogeneity clearly makes it more suitable for obtaining sizes in heterogeneous specimens. However, here, where severe magnetic susceptibility effects prevail, it is even more important to concatenate the d-PFG sequence with bipolar gradients. It should be noted that in many realistic porous media, even the presence of restricted diffusion is hard to determine, especially if the signal decays rapidly due to susceptibility effects. Detection of zero-crossings is therefore advantageous since it provides unequivocal evidence for the presence of restricted diffusion within the porous medium.

In the present study, we have also shown, for the first time, that compartment shape anisotropy can be inferred from the $E(\psi)$ plots in angular bp-d-PFG experiments with long mixing times. The angle ψ adds another dimension which is unique to d-PFG, and has no analogs in s-PFG methodologies. Rather than plotting $E(q)$ profiles, the angu-

lar d-PFG experiments yield $E(\psi)$ profiles for different values of q , from which local compartment shape anisotropy can be calculated.²⁹ At long mixing times (t_m), the compartment shape anisotropy is decoupled from microscopic anisotropy that may be present,²⁹ and the $E(\psi)$ profile can be used to differentiate between spherical and nonspherical pores:²⁹ while $E(\psi)$ was predicted to be flat for spherical pores, characteristic modulated curves should be obtained for other compartment shapes. In this study, we clearly observed the modulation in $E(\psi)$, thus we could directly infer that our randomly oriented compartments were indeed nonspherical. In other studies,^{31,33} we studied the long t_m behavior in a pack of coherently placed cylinders, where a flat behavior of $E(\psi)$ was observed. Interestingly, the angular d-PFG experiment was performed there on a perimeter of a circle (since the pores were coherently placed and the angular d-PFG was performed in the plane perpendicular to the main axis of the pores^{31,33}), which has the same compartment shape anisotropy as a sphere; therefore, the flat angular dependence is consistent with that expected of diffusion in a sphere. Other studies^{26,27} compared $E(q)$ data at two different values of ψ to infer on locally anisotropic motion; however, such measurements rely just on two points in the $E(\psi)$ curves that may be influenced, for example, by the susceptibility effects. Thus, observing the full $E(\psi)$ modulation at different q -values offers a much more robust and quantitative means for measuring compartment shape anisotropy even at low q -values.²⁹ In the present study, the full modulated bell shaped functions at long t_m were observed for the first time, unequivocally demonstrating that while overall diffusion is isotropic, the local anisotropy of the pores can be inferred directly from the $E(\psi)$ plots. This inherent attribute of d-PFG MR can become important in characterizing other porous media including porous materials, pores in rocks, and even gray matter in the CNS.

It should be noted that in addition to compartment shape, accurate compartment size can also be extracted from the $E(\psi)$ plots, albeit not as directly as using the zero-crossings as signatures for compartment size.^{30,31,43} However, another advantage of acquiring $E(\psi)$ plots is that relatively low- q values can be used, and therefore the signal to noise ratio is high. Compartment shape anisotropy in this study was, in fact, observed at low q -values, comparable with q -values in which DTI is routinely performed in the clinic; therefore, our findings imply that using bp-d-PFG in imaging to create shape contrasts in CNS structures should be feasible.

A unique property of our randomly oriented specimens is the complete lack of exchange of water between intra- and extratubular spaces. Although the water-filled anisotropic pores are randomly oriented and open on both ends, the polarity differences between the extratubular Fluorinert and intratubular water preclude any water exchange between compartments. The lack of exchange is advantageous for the objectives of this study, which were to validate the theory and challenge the accuracy of the extracted microstructural information. It should be noted that other approaches employing, for example, two-dimensional acquisition schemes, indeed addressed the matter of exchange.^{24,45-47} Angular d-PFG studies may indeed become important in studying ex-

change phenomena since the angular dependence arises only when restricted diffusion occurs, in contrast with multiexponential Gaussian processes.^{43,30}

The random orientation of the compartments in our study resulted in relatively large susceptibility artifacts, which were manifested in a relatively large linewidth (~ 0.5 kHz). Importantly, susceptibility effects in porous materials such as rocks and other porous media¹⁸ are usually large, and susceptibility mechanisms are now being extensively studied as new sources of contrast in magnetic resonance imaging (MRI) of the CNS.⁴⁸ In this study, we were able to show that the bp-d-PFG methodologies can yield zero-crossings and bell shaped functions despite this large susceptibility effects in the sample. These findings imply that bp-d-PFG can be advantageous in a wide range of applications.

Finally, we note that the bp-d-PFG sequences used in this study are relatively simple in terms of MR sequences and can be easily implemented. Coupled to its ability to convey pore size and shape, it is clear that bp-d-PFG is the method of choice for studying heterogeneous porous systems of paramount importance in both applied and basic science.

ACKNOWLEDGMENTS

P.J.B. and E.Ö. were supported by the Intramural Research Program of the Eunice Kennedy Shriver National Institute of Child Health and Human Development, NIH. Y.C. and N.S. were partially supported by the CONNECT consortium administered by the European Commission under Framework Package 7.

- ¹ P. N. Sen, *J. Phys.: Condens. Matter* **16**, S5213 (2004).
- ² Y. Q. Song, H. Cho, T. Hopper, A. E. Pomerantz, and P. Z. Sun, *J. Chem. Phys.* **128**, 052212 (2008).
- ³ Y. Q. Song, S. G. Ryu, and P. N. Sen, *Nature (London)* **406**, 178 (2000).
- ⁴ V. Kukla, J. Kornatowski, D. Demuth, I. Gimus, H. Pfeifer, L. V. C. Rees, S. Schunk, K. K. Unger, and J. Kärger, *Science* **272**, 702 (1996).
- ⁵ R. Valiullin, S. Naumov, P. Galvosas, J. Kärger, H.-J. Woo, F. Porcheron, and P. A. Monson, *Nature (London)* **443**, 965 (2006).
- ⁶ B. Hakansson, R. Pons, and O. Söderman, *Magn. Reson. Imaging* **16**, 643 (1998).
- ⁷ G. Pages, D. Szekely, and P. W. Kuchel, *J. Magn. Reson. Imaging* **28**, 1409 (2008).
- ⁸ D. Le Bihan, *Nat. Rev. Neurosci.* **4**, 469 (2003).
- ⁹ E. O. Stejskal and J. E. Tanner, *J. Chem. Phys.* **42**, 288 (1965).
- ¹⁰ P. J. Basser, J. Mattiello, and D. LeBihan, *J. Magn. Reson., Ser. B* **103**, 247 (1994).
- ¹¹ P. J. Basser and D. K. Jones, *NMR Biomed.* **15**, 456 (2002).
- ¹² S. Mori, B. J. Crain, V. P. Chacko, and P. C. M. van Zijl, *Ann. Neurol.* **45**, 265 (1999).
- ¹³ M. A. Horsfield and D. K. Jones, *NMR Biomed.* **15**, 570 (2002).
- ¹⁴ P. T. Callaghan, A. Coy, D. Macgowan, K. J. Packer, and F. O. Zelaya, *Nature (London)* **351**, 467 (1991).
- ¹⁵ L. Avram, E. Özarslan, Y. Assaf, A. Bar-Shir, Y. Cohen, and P. J. Basser, *NMR Biomed.* **21**, 888 (2008).
- ¹⁶ P. W. Kuchel, A. Coy, and P. Stilbs, *Magn. Reson. Med.* **37**, 637 (1997).
- ¹⁷ Y. Q. Song, *J. Magn. Reson.* **143**, 397 (2000).
- ¹⁸ M. D. Hürlimann, *J. Magn. Reson.* **131**, 232 (1998).
- ¹⁹ P. N. Sen and S. Axelrod, *J. Appl. Phys.* **86**, 4548 (1999).
- ²⁰ G. Zheng and W. S. Price, *Concepts Magn. Reson. A* **30A**, 261 (2007).
- ²¹ A. Bar-Shir and Y. Cohen, *Magn. Reson. Imaging* **26**, 801 (2008).
- ²² K. G. Hollingsworth, A. J. Sederman, C. Buckley, L. F. Gladden, and M. L. Johns, *J. Colloid Interface Sci.* **274**, 244 (2004).
- ²³ D. G. Cory, A. N. Garraway, and J. B. Miller, *Polym. Prepr. (Am. Chem. Soc. Div. Polym. Chem.)* **31**, 149 (1990).
- ²⁴ P. T. Callaghan and I. Furo, *J. Chem. Phys.* **120**, 4032 (2004).

- ²⁵ A. Jerschow and N. Muller, *J. Magn. Reson.* **125**, 372 (1997).
- ²⁶ Y. Cheng and D. G. Cory, *J. Am. Chem. Soc.* **121**, 7935 (1999).
- ²⁷ P. T. Callaghan and M. E. Komlosh, *Magn. Reson. Chem.* **40**, S15 (2002).
- ²⁸ E. Özarslan and P. J. Basser, *J. Magn. Reson.* **188**, 285 (2007).
- ²⁹ E. Özarslan, *J. Magn. Reson.* **199**, 56 (2009).
- ³⁰ E. Özarslan and P. J. Basser, *J. Chem. Phys.* **128**, 154511 (2008).
- ³¹ E. Özarslan, N. Shemesh, and P. J. Basser, *J. Chem. Phys.* **130**, 104702 (2009).
- ³² N. Shemesh and Y. Cohen, *J. Magn. Reson.* **195**, 153 (2008).
- ³³ N. Shemesh, E. Özarslan, P. J. Basser, and Y. Cohen, *J. Magn. Reson.* **198**, 15 (2009).
- ³⁴ N. Shemesh, E. Özarslan, A. Bar-Shir, P. J. Basser, and Y. Cohen, *J. Magn. Reson.* **200**, 214 (2009).
- ³⁵ N. Shemesh, E. Özarslan, P. J. Basser, and Y. Cohen, *J. Chem. Phys.* **132**, 034703 (2010).
- ³⁶ M. E. Komlosh, F. Horkay, R. Z. Freidlin, Y. Assaf, and P. J. Basser, Proceedings of the Seventh ENC, 2006, Paper No. E060077.
- ³⁷ M. E. Komlosh, F. Horkay, R. Z. Freidlin, U. Nevo, Y. Assaf, and P. J. Basser, *J. Magn. Reson.* **189**, 38 (2007).
- ³⁸ M. E. Komlosh, M. J. Lizak, F. Horkay, R. Z. Freidlin, and P. J. Basser, *Magn. Reson. Med.* **59**, 803 (2008).
- ³⁹ M. A. Koch and J. Finsterbusch, *Magn. Reson. Med.* **60**, 90 (2008).
- ⁴⁰ T. Weber, C. H. Ziener, T. Kampf, V. Herold, W. R. Bauer, and P. M. Jakob, *Magn. Reson. Med.* **61**, 1001 (2009).
- ⁴¹ T. J. Larkin and P. W. Kuchel, *Eur. Biophys. J.* **39**, 139 (2009).
- ⁴² L. Ambrosone, A. Ceglie, G. Colafemmina, and G. Palazzo, *J. Chem. Phys.* **107**, 10756 (1997).
- ⁴³ P. P. Mitra, *Phys. Rev. B* **51**, 15074 (1995).
- ⁴⁴ P. Z. Sun, J. G. Seland, and D. Cory, *J. Magn. Reson.* **161**, 168 (2003).
- ⁴⁵ M. I. Menzel, S. Han, S. Stapf, and B. Blümich, *J. Magn. Reson.* **143**, 376 (2000).
- ⁴⁶ R. G. Graham, W. H. Holmes, C. De Panfilis, and K. J. Packer, *Chem. Phys. Lett.* **332**, 319 (2000).
- ⁴⁷ P. T. Callaghan, C. H. Arns, P. Galvosas, M. W. Hunter, Y. Qiao, and K. E. Washburn, *Magn. Reson. Imaging* **25**, 441 (2007).
- ⁴⁸ J. Lee, K. Shmueli, M. Fukunaga, P. van Gelderen, H. Merkle, A. C. Silva, and J. H. Duyn, *Proc. Natl. Acad. Sci. U.S.A.* **107**, 5130 (2010).